

## ***Q* factor estimation based on the method of logarithmic spectral area difference**

Shoudong Wang<sup>1</sup>, Dengfeng Yang<sup>2</sup>, Jingnan Li<sup>3</sup>, and Huijuan Song<sup>4</sup>

### **ABSTRACT**

We have developed a novel method for  $Q$  estimation. As a seismic wave propagates through subsurface viscoelastic media, seismic attenuation decreases the amplitude and reduces the bandwidth, which leads to variation of the logarithmic spectral area of seismic wave. According to this property, we have derived an analytical relation between  $Q$  factor and the logarithmic spectral area difference of seismic wave. To improve the accuracy of  $Q$  estimation, we took account of the amplitude loss due to energy partitioning from transmission. Tests of the method on synthetic models determined the validity of our method, and it was insensitive to different types of noises and evaluated

density. A further comparison between the presented method and two widely used  $Q$  estimation methods, namely, the logarithmic spectral ratio and centroid frequency shifting methods, with a synthetic model containing random noise demonstrated that our method is the more robust, in these situations, among the three approaches. Then, we also compared the effect of bandwidth and time-window selection on the  $Q$  estimation for these three methods, and the result revealed that our method is less sensitive to the bandwidth and time window than the other two methods. Application of this method to real zero-offset vertical seismic profile data shows a reasonable correlation between estimated interval- $Q$  and interval velocities, which further indicates the validity of the method.

### **INTRODUCTION**

Attenuation, which can be parameterized by the  $Q$  factor, decreases the resolution of seismic data. On the other hand, it makes the imaging and interpretation of the subsurface more difficult. Fortunately, reliable estimate of the viscoelastic attenuation can help to improve the resolution of seismic data through inverse  $Q$ -filtering (Wang, 2006) and to precisely image subsurface by incorporating attenuation into migration (Mittet et al., 1995). In addition, a better interpretation of the subsurface structure can be achieved by the joint inversion of velocity and  $Q$  values (Liao and McMechan, 1996; Hicks and Pratt, 2001). Furthermore,  $Q$  itself is a useful parameter because it is sensitive to parameters, such as lithology, porosity, and pore-fluid characteristics (Johnston et al., 1979; Best,

1997). For instance, attenuation is intense in gas saturation (Winkler and Nur, 1982), and the magnitude of attenuation change with azimuth can be used to indicate the fracture direction (Clark et al., 2001; Maultzsch et al., 2007; Rao and Wang, 2009). Therefore,  $Q$  estimation plays a vital role in seismic data processing.

Several groups have studied  $Q$  factor measurements. Tonn (1991) investigates 10 methods for the computation of attenuation and proves that no single method is generally superior. Each method has advantages as well as limitations. He demonstrates that the spectral ratio method was optimal in the noise-free case but is very sensitive to noise. Subsequently,  $Q$  estimation methods based on the change of signal frequency have been proposed. Quan and Harris (1997) present the frequency shift method to estimate seismic attenuation, in which the incident spectrum was assumed Gaussian,

Manuscript received by the Editor 30 May 2014; revised manuscript received 19 March 2015; published online 26 August 2015.

<sup>1</sup>China University of Petroleum (Beijing), State Key Laboratory of Petroleum Resource and Prospecting; National Engineering Laboratory of Offshore Oil Exploration; CNPC Key Laboratory of Geophysical Exploration, Beijing, China. E-mail: ctlab@cup.edu.cn.

<sup>2</sup>Formerly China University of Petroleum (Beijing), State Key Laboratory of Petroleum Resource and Prospecting; National Engineering Laboratory of Offshore Oil Exploration, Beijing, China; presently The Research Institute of CNOOC (China) Ltd, Shenzhen, China. E-mail: yangdfdqwl@163.com.

<sup>3</sup>China University of Petroleum (Beijing), State Key Laboratory of Petroleum Resource and Prospecting; CNPC Key Laboratory of Geophysical Exploration, Beijing, China. E-mail: li.jinan@163.com.

<sup>4</sup>Formerly China University of Petroleum (Beijing), State Key Laboratory of Petroleum Resource and Prospecting; National Engineering Laboratory of Offshore Oil Exploration, Beijing; presently Jianghan Branch of Sinopac Geophysical Corporation, Qianjiang, China. E-mail: songhj\_wish@163.com.

© 2015 Society of Exploration Geophysicists. All rights reserved.

boxcar, or triangular shape. Zhang and Ulrych (2002) find that the interval  $Q$  factor could be computed solely from the variation of the peak frequency of a spectrum as a function of time, when the amplitude spectrum of a seismic wavelet was supposed to be Ricker-like. Some other methods for  $Q$  estimation using the time-frequency analysis techniques can also be referenced. Because of the spectral interference of reflection seismic data, the measurement of  $Q$  may be unstable. To stably estimate  $Q$  from reflection seismic data, two  $Q$ -analysis methods based on amplitude attenuation and compensation functions with Gabor transform were proposed (Wang, 2004). Meanwhile, to remove local thin-bed effects, Hackert and Parra (2004) propose the method of well log-based localized spectral correction to improve  $Q$  estimates from seismic reflection data. Besides, Reine et al. (2009) compare four time-frequency transforms for  $Q$  estimation, namely, the short-time Fourier transform, continuous wavelet transform, Gabor transform, and S-transform. They found that variable-window transforms reduced the uncertainty and bias of the resulting attenuation. Reine et al. (2012a, 2012b) successfully develop a prestack  $Q$ -inversion technique for measuring attenuation from prestack surface seismic gathers. The presence of spectral interference can be minimized by combining the variable window time-frequency transform with an inversion scheme operating simultaneously in the frequency and traveltime-difference coordinates. Recently, the application of optimization theory to  $Q$  estimation has become an important development trend. For example, the velocity and  $Q$  can be reconstructed jointly by full-waveform inversion method in frequency domain (Liao and McMechan, 1996; Hicks and Pratt, 2001; Malinowski et al., 2011). Moreover, Blas (2012) suggests an optimization approach to  $Q$  estimation based on the conventional absorption model. In general, these optimization methods are more accurate but yet more computationally expensive.

In this paper, we present a new method for  $Q$  estimation. Attenuation can decrease the amplitude and reduce the bandwidth; it then leads to the variation of the logarithmic spectral area of seismic wave. On the basis of this property, we establish the analytical relation between  $Q$  factor and logarithmic spectral area difference (LSAD) of seismic wave. Numerical tests, comparative analysis of different  $Q$  estimation methods and real zero-offset vertical seismic profile (VSP) data processing indicate that the presented method can estimate  $Q$  stably and effectively, and also has good noise immunity.

## METHODS

### $Q$ estimation based on the logarithmic spectral area difference

We consider the problem of wave propagation in attenuating media characterized by the causal constant  $Q$  model of Futterman (1962) as given by

$$\begin{aligned} \bar{A}(z_{i+1}, \omega) &= PG \cdot \bar{A}(z_i, \omega) \exp\left[-\frac{\omega \Delta z_i}{2Q_i v(z_i, \omega)}\right] \\ &\times \exp\left[-i\omega \frac{\Delta z_i}{v(z_i, \omega)}\right], \end{aligned} \quad (1)$$

where  $P$  indicates the amplitude losses due to energy partitioning from reflection and transmission at impedance interfaces,  $G$  stands

for geometric spreading. The  $\bar{A}(z_i, \omega)$  is the frequency spectra at depth  $z_i$ ,  $v(z_i, \omega)$  is the frequency-dependent phase velocity,  $Q_i$  is the quality factor for the depth  $(z_i, z_{i+1})$ ,  $\Delta z_i = z_{i+1} - z_i$  is the travel distance, and  $\omega$  is the circular frequency. We use the model described by Wang (2002), the relation among velocity, frequency, and quality factor can be defined by

$$\begin{aligned} v(z_i, \omega) &= v(z_i, \omega_0) \left| \frac{\omega}{\omega_0} \right|^{\gamma} \quad \text{and} \\ \gamma &= \frac{2}{\pi} \tan^{-1} \left( \frac{1}{2Q_i} \right) \approx \frac{1}{\pi Q_i}, \end{aligned} \quad (2)$$

where  $v(z_i, \omega_0)$  is the phase velocity corresponding to dominant frequency  $\omega_0$ .

Considering only the amplitude spectra and assuming that propagation velocity is frequency independent within seismic bandwidth, equation 1 can be simplified as

$$A(z_{i+1}, \omega) = PG \cdot A(z_i, \omega) \exp\left[-\frac{\omega \Delta t_i}{2Q_i}\right], \quad (3)$$

where  $\Delta t_i = \frac{\Delta z_i}{v(z_i, \omega_0)}$ ,  $A(z_i, \omega)$  is the amplitude spectra at depth  $z_i$ .

Then, we rewrite equation 3 as a linear equation:

$$\ln[A(z_{i+1}, \omega)] = \ln[A(z_i, \omega)] - \frac{\omega \Delta t_i}{2Q_i} + \ln(PG). \quad (4)$$

Equation 4 can also be expressed as

$$\ln\left[\frac{A(z_{i+1}, \omega)}{A(z_i, \omega)}\right] = -\frac{\omega \Delta t_i}{2Q_i} + \ln(PG). \quad (5)$$

Calculating the  $Q$  factor according to equation 5 is referred to as *logarithmic spectral ratio* (LSR) method. Then, the least-squares linear regression is often used in the LSR method in a selected frequency band. The  $Q$  value is estimated from the slope of a straight line fit to the logarithmic ratio of two spectrums. A main limitation of the LSR method is its sensitivity to random noise (Tonn, 1991).

Suppose that the mean value of the errors of logarithmic spectra caused by random noise approximately equals zero. Then we can reduce the effect of random noise with an integral operation on the logarithmic spectra, for the reason that the integral operation is equivalent to the summation. Attenuation decreases the amplitude and reduces the bandwidth; it then leads to the variation of the logarithmic spectral area of seismic wave. The calculation of the logarithmic spectral area is just an integral operation. If we define the logarithmic spectral area, which is the definite integral of the function of logarithmic spectrum with a given frequency interval  $[\omega_{\min}, \omega_{\max}]$ ,  $S(z)$ , at depth  $z$  as

$$S(z) = \int_{\omega_{\min}}^{\omega_{\max}} \ln[A(z, \omega)] d\omega, \quad (6)$$

thus, we can obtain the LSAD between two receivers as follows:

$$\Delta S_i = S(z_i) - S(z_{i+1}). \quad (7)$$

For the zero-offset VSP data,  $Q$  is estimated using the first arrivals of the downgoing transmission waves. To accurately estimate interval- $Q$  from the zero-offset VSP data, we must first eliminate the impact of transmission. With regard to zero-offset data, the interval velocity  $v_i$  can be calculated from the first arrivals. According to the Gardner et al. (1974) empirical equation,  $\rho = 0.31 \times v_p^{\frac{1}{3}}$ , the density  $\rho_i$  can also be obtained, where  $v_p$  is the primary velocity. For simplicity, the coefficient  $P$  in equation 4 can only be regarded as the amplitude losses due to energy partitioning from transmission for the first arrivals. Then,  $P$  is equivalent to the transmission coefficient, which can be calculated by

$$P_i = \frac{2\rho_i v_i}{\rho_{i+1} v_{i+1} + \rho_i v_i}. \quad (8)$$

After the correction of the geometric divergence effect for the first arrivals, which removes the  $G$  in the equation 4, we rewrite equation 4 as

$$\ln[A(z_{i+1}, \omega)] = \ln[A(z_i, \omega)] - \frac{\omega \Delta t_i}{2Q_i} + \ln(P_i). \quad (9)$$

According to equations 6 and 9, we can rewrite equation 7 as

$$\begin{aligned} \Delta S_i &= \int_{\omega_{\min}}^{\omega_{\max}} \ln[A(z_i, \omega)] d\omega - \int_{\omega_{\min}}^{\omega_{\max}} \ln[A(z_{i+1}, \omega)] d\omega, \\ &= \int_{\omega_{\min}}^{\omega_{\max}} \ln[A(z_i, \omega)] d\omega \\ &\quad - \int_{\omega_{\min}}^{\omega_{\max}} \left\{ \ln[A(z_i, \omega)] - \frac{\omega \Delta t_i}{2Q_i} + \ln(P_i) \right\} d\omega, \\ &= \int_{\omega_{\min}}^{\omega_{\max}} \frac{\omega \Delta t_i}{2Q_i} d\omega - \int_{\omega_{\min}}^{\omega_{\max}} \ln(P_i) d\omega. \end{aligned} \quad (10)$$

In terms of equation 10, a new formula for  $Q$  estimation is expressed as

$$Q_i = \frac{\Delta t_i}{2[\Delta S_i + \int_{\omega_{\min}}^{\omega_{\max}} \ln(P_i) d\omega]} \int_{\omega_{\min}}^{\omega_{\max}} \omega d\omega. \quad (11)$$

In the present paper,  $Q$  estimation based on equation 11 is called the *method of LSAD*.

### Interval- $Q$ estimation from average- $Q$

In seismic data processing,  $Q$  estimation procedure is akin to the conventional velocity analysis. Once a series of average- $Q$  factors are obtained, we can calculate a series of interval- $Q$  factors. Suppose that the earth is divided into  $N$  layers with interval- $Q$  factors,  $\{Q_1, \dots, Q_N\}$ . The location of the shallowest receiver is at time  $T_0 = 0$ , regarded as a reference level. According to equation 3, after attenuation the amplitude of the  $n$ th receiver can be expressed as

$$A(z_n, \omega) = \left( \prod_{i=1}^{n-1} P_i \right) \cdot A(z_1, \omega) \exp \left[ -\sum_{i=1}^{n-1} \frac{\omega \Delta t_i}{2Q_i} \right]. \quad (12)$$

The average- $Q$  factors can be obtained by

$$\frac{1}{(Q_a)_n} = \frac{1}{T_n} \sum_{i=1}^n \frac{1}{Q_i} \Delta t_i \quad \text{and} \quad \frac{1}{(Q_a)_{n-1}} = \frac{1}{T_{n-1}} \sum_{i=1}^{n-1} \frac{1}{Q_i} \Delta t_i, \quad (13)$$

where  $(Q_a)_n$  and  $(Q_a)_{n-1}$  are average- $Q$  calculated at time  $T_n = \sum_{i=1}^n \Delta t_i$  and  $T_{n-1} = \sum_{i=1}^{n-1} \Delta t_i$ , respectively. Then, the interval- $Q$  for the  $n$ th layer is given by

$$\frac{1}{Q_n} = \frac{T_n/(Q_a)_n - T_{n-1}/(Q_a)_{n-1}}{T_n - T_{n-1}}. \quad (14)$$

Based on equation 11, the average- $Q$  for the  $n-1$  layers can be estimated by

$$(Q_a)_{n-1} = \frac{T_{n-1}}{2[(\Delta S_a)_n + \int_{\omega_{\min}}^{\omega_{\max}} \ln(\prod_{i=1}^{n-1} P_i) d\omega]} \int_{\omega_{\min}}^{\omega_{\max}} \omega d\omega, \quad (15)$$

where  $(\Delta S_a)_n = S(z_1) - S(z_n)$ .

## NUMERICAL TESTS

In this section, we first analyze the validity and noise immunity of the proposed method through a synthetic attenuation model. Then, we examine the effect of density uncertainty on  $Q$  estimation based on LSAD. Nevertheless, in addition to the factors mentioned above, a lot of other factors, such as random noise, bandwidth, and the time window, also affect  $Q$  measurements. To illustrate the superiority of our method, we compare the sensitivity of LSAD and another two methods, namely LSR and centroid frequency shifting (CFS), to these above factors.

### Effectiveness and noise-immunity analysis of the logarithmic spectral area difference

In this section, we examine the effectiveness and noise immunity of LSAD through a synthetic attenuation model. A two-layer model is given, and the parameters of this model are shown in Figure 1.

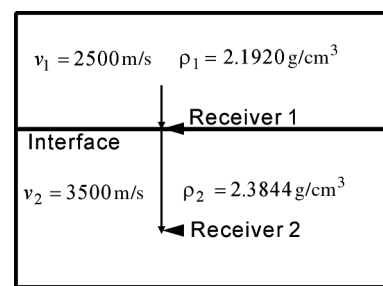


Figure 1. A two-layer model with parameters and downgoing wave-propagation scheme.

Suppose that a Ricker wavelet with 45-Hz dominant frequency, the reference wavelet, is vertically incident to the interface, and it is recorded by the first receiver, which is located at the interface. Then, the wavelet transmits through the interface and is recorded by the second receiver. The traveltime between the two receivers is 300 ms. And these two received signals are shown in a same trace. Figure 2a depicts a synthetic attenuation model with different  $Q$  ( $Q = 20, 40, 80$ , and  $160$ , respectively) of the second layer. Assume that the density can be obtained accurately when we verify the validity of LSAD. The selected frequency band of LSAD is 10–100 Hz, and the width of time window is 70 ms. The estimated  $Q$  (see Figure 2b) from noise-free data shows good agreement with the actual  $Q$ , which confirms the validity of our method.

Then, Gaussian random noise of 5%, 10%, and 15% of maximum amplitude of the reference wavelet is added to the noise-free traces, which are shown in Figure 3. For  $Q$  estimation on the basis of LSAD, 200 independent runs are carried out with different additive

Gaussian random noises. Then, the mean values and standard deviations of the estimated  $Q$  from the synthetic model with different Gaussian random noise are indicated in Figure 4. According to the result, the estimated  $Q$  mean values (shown in Figure 4a) are close to the true values, and the standard deviations are very small in different attenuation situations in which the data are with 5% Gaussian random noise. And even for the case with 10% and 15% Gaussian random noise, the calculated  $Q$  mean values and standard deviations, displayed in Figure 4b and 4c separately, are reasonable. Moreover, for purposes of testing the impact of the noise type on the proposed method, we also add different levels of Cauchy random noises to the noise-free data, and the evaluated results are shown in Figure 5. Also, the mean values and standard deviations of  $Q$  estimated from the synthetic model with different Cauchy random noises are depicted in Figure 6. The results of Figures 4 and 6 together demonstrate that the LSAD method has good noise immunity to different types of random noises.

Figure 2. (a) The synthetic attenuation model with different  $Q$  ( $Q = 20, 40, 80$ , and  $160$ , respectively) of the second layer. (b) The corresponding estimated  $Q$  using the LSAD method.

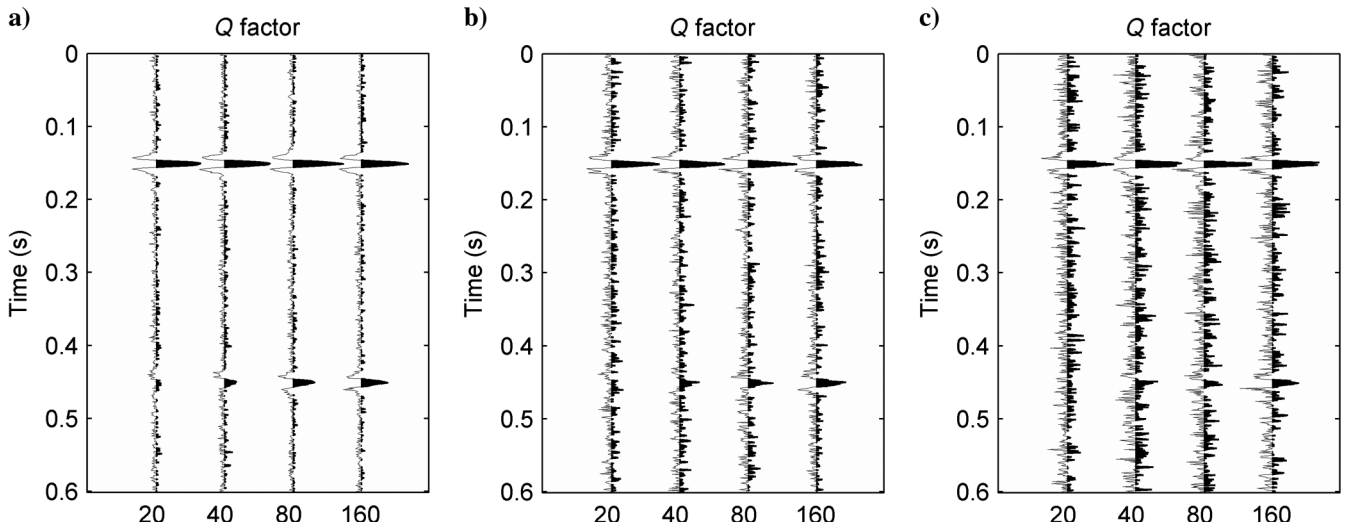
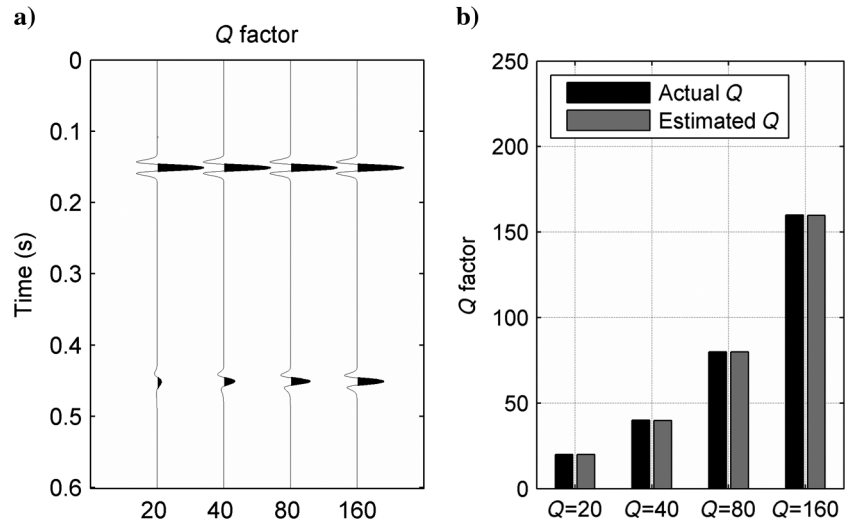


Figure 3. The synthetic attenuation model with different levels of Gaussian random noise: (a) 5% Gaussian random noise, (b) 10% Gaussian random noise, and (c) 15% Gaussian random noise.

In addition, we give an error analysis on the LSAD method in Appendix A, which explains the robust of our method for  $Q$  estimation in detail when the data contain random noise.

### The density sensitivity analysis of the logarithmic spectral area difference

In our method, the transmission coefficient is considered, as shown in equation 11; thus, we need to know the interval velocities and the corresponding densities of every layer. The former can be obtained from the first arrivals for zero-offset VSP data, whereas the latter are calculated using the Gardner equation. Because it is an empirical equation, the calculated densities probably deviate from true ones, and this will cause an error on the transmission coeffi-

cient, which will affect the accuracy of the  $Q$  estimation. So, we examine the effect of uncertainty in density on  $Q$  estimation using LSAD in this section.

The synthetic attenuation model (Figure 2a) is used to analyze the density sensitivity of LSAD. The selected frequency band of LSAD is 10–100 Hz, and the width of the time window is 70 ms. First, we assume that the layered velocity and the density of the first layer are known. The obtained density of the second layer using the Gardner equation has some errors. The corresponding relative errors of the transmission coefficient caused by density bias are counted and shown in Figure 7a. (Assume that  $A$  is the true value and  $B$  is the estimated value. Then, the relative error  $E_R$  can be defined as  $E_R = \frac{B-A}{A}$ .) And the relative errors of the estimated  $Q$  are indicated in Figure 7b. Second, we assume that the obtained density of

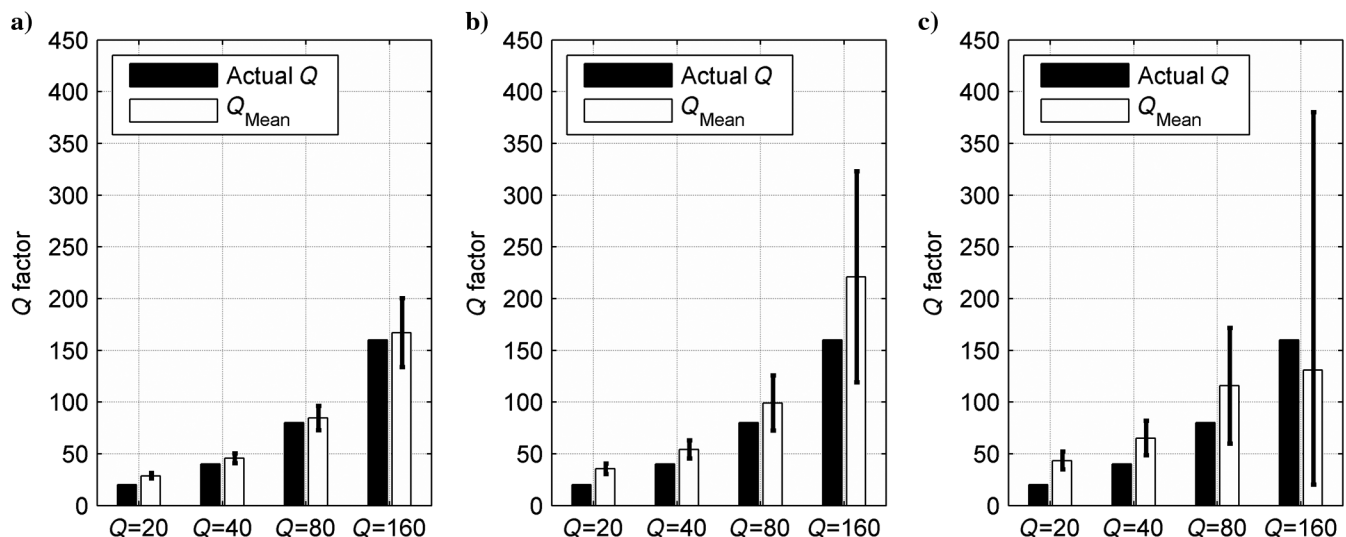


Figure 4. The corresponding estimated  $Q$  mean values and standard deviations using the LSAD method from the noisy models of Figure 3. The white bar denotes the estimated mean value, the black bar represents the actual  $Q$ , and the black H-shaped line represents the standard deviation. Cases of (a) 5%, (b) 10%, and (c) 15% Gaussian random noise.

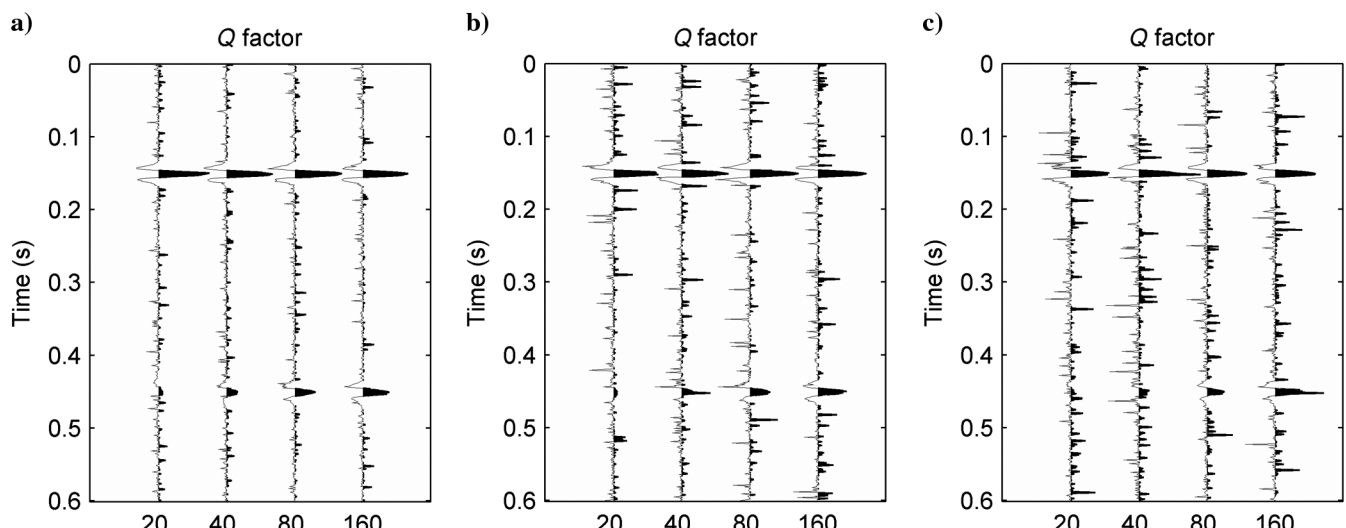


Figure 5. The synthetic attenuation model with different levels of Cauchy random noise: (a) 5%, (b) 10%, and (c) 15% Cauchy random noise.

the second layer is accurate, and the density of the first layer is inaccurate. Then, in a similar way, the relative errors of the transmission coefficient and the relative errors of the estimated  $Q$  are acquired and displayed in Figure 8a and 8b, respectively.

According to Figures 7 and 8, it is noticeable that the estimated  $Q$  value is less than the true value when the relative error of the transmission coefficient is greater than zero, and it is greater than the true value when the relative error of the transmission coefficient is less than zero. In detail, if the relative error of transmission coefficient is less than 10% or larger than -10%; i.e., the relative error of calculated density is less than 15% or larger than -15%, and the relative errors of the estimated  $Q$  are not greater than 50% or less than -50% when the true attenuation is relatively large. We

can also find that the stronger the attenuation is, the less sensitive to density the method is. For example, even for the relative error of calculated density being -25%, the relative error of estimated  $Q$  ( $Q = 20$  or  $40$ ) is less than -15%. However, if the relative error of density is greater than -15% or less than 15% and the actual  $Q$  is large, e.g.,  $Q = 160$ , the estimated  $Q$  based on LSAD is unacceptable.

### Comparative analysis of noise-immunity of three $Q$ estimation methods

In this section, we compare the sensitivity of three  $Q$  estimation methods to random noise, that is,  $Q$  estimation with LSAD, LSR,

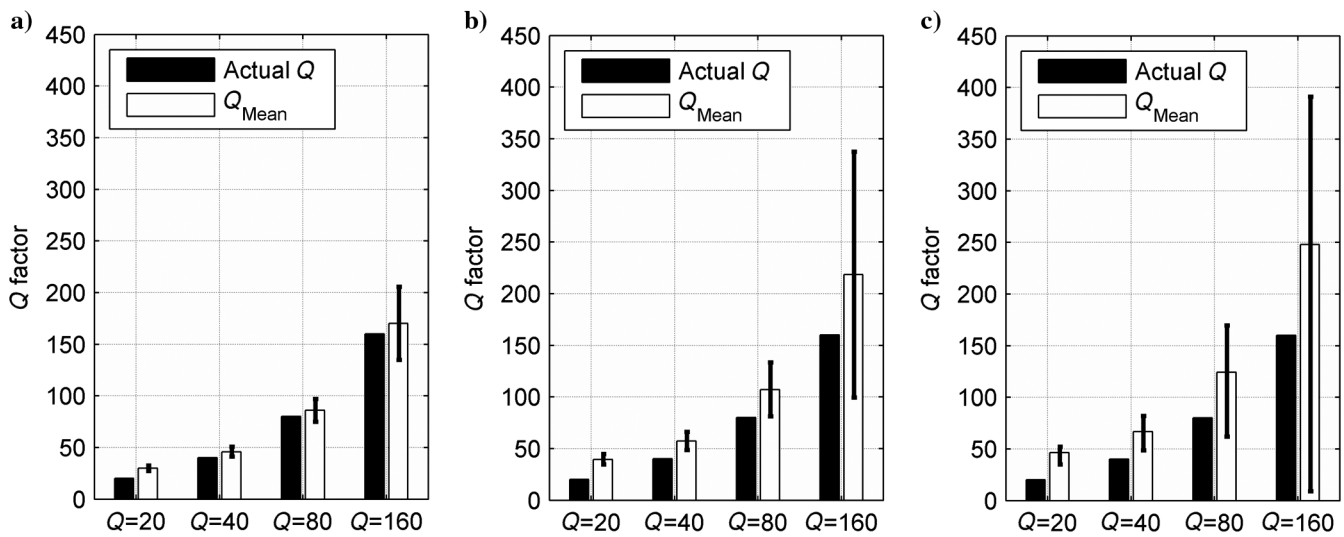


Figure 6. The corresponding estimated  $Q$  using the LSAD method from the noisy models of Figure 5. The white bar denotes the estimated mean value, the black bar represents the actual  $Q$ , and the black H-shaped line represents the standard deviation. Cases of (a) 5%, (b) 10%, and (c) 15% Cauchy random noise.

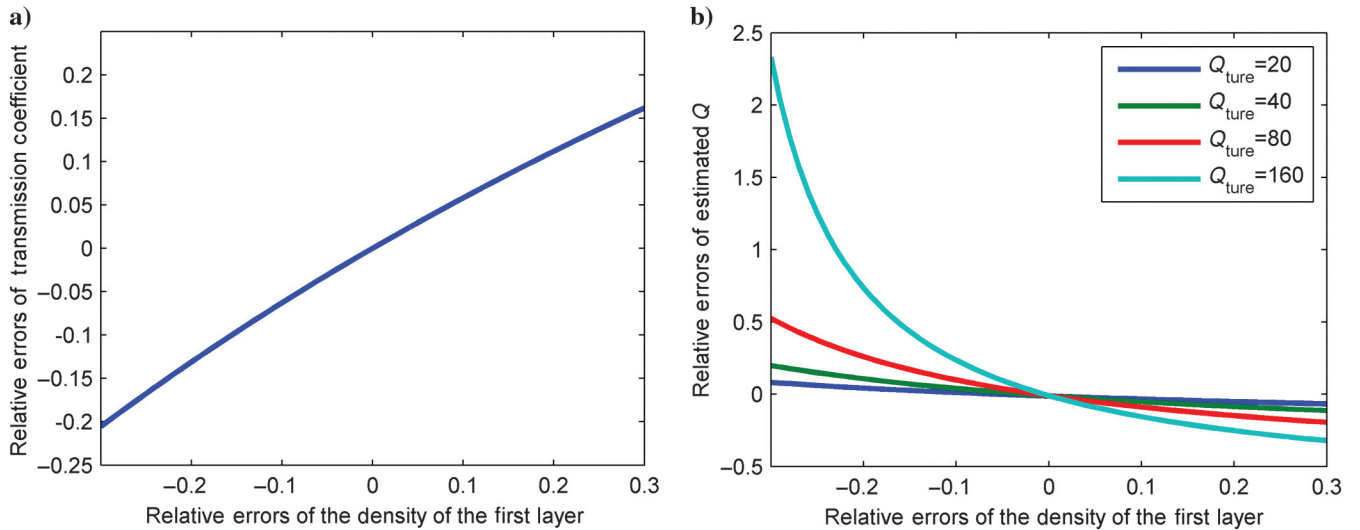


Figure 7. (a) The corresponding relative errors of the transmission coefficient caused by the computed density of the first layer. (b) The relative errors of the estimated  $Q$ .

and CFS. The second trace ( $Q = 40$ ) of the synthetic attenuation model (Figure 2a) is selected for our tests. The signature spectra before and after attenuation, from which we can calculate the centroid frequencies, are shown in Figure 9. And we can evaluate  $Q$  from the shift of centroid frequency by the CFS method. In Figure 10, the logarithmic spectrum ratio that is used to estimate  $Q$  in the LSR method, are obtained using the wavelet spectra before and after attenuation. Figure 11 depicts the LSAD, marked in the gray section, which we use to estimate  $Q$  in terms of the LSAD approach.

For  $Q$  measurement, 200 independent realizations are carried out with different additive Gaussian random noises. The selected frequency band of these three methods is 10–100 Hz, and the time window width is 70 ms. Figure 12 illustrates the estimated  $Q$  with different methods when the additive Gaussian random noise is 5%. The probability distributions of  $Q$  estimation using LSAD for an accurate transmission coefficient, transmission coefficient with -50% relative error, and that with 15% relative error are shown in Figure 12a–12c, respectively. Figure 12d and 12e is the statistical performance of estimated  $Q$  with LSR and CFS, respectively. In the case of 10% and 15% Gaussian random noise, the corresponding statistical results are displayed in Figures 13 and 14, respectively. The mean and the variance are also given in all these figures, in which “Mean” and “Var” stand for the mean and variance of estimated  $Q$  values, respectively.

In Figure 12, we can see that the histograms for LSAD show a more peaked distribution compared with those of LSR and CFS. The histograms in Figures 13 and 14 reveal the same results. Conversely, the histograms of LSR and CFS indicate a larger variability in results, and they include the estimated  $Q$  values farther from the central peak. Especially in Figure 14, there are almost no central peaks for LSR and CFS and the variances are as large as  $4.33 \times 10^7$  and  $2.5 \times 10^5$ , respectively, which demonstrates that the estimated  $Q$  is unstable and unacceptable at this level of random noise. Comparing the mean values in these figures, it is obviously seen that the estimated  $Q$  values using LSAD are closest to the true values. Even for the transmission coefficient with relative

error -15% or 15%, the calculated mean values with LSAD are still more accurate than those with LSR and CFS. According to these statistical performances of estimated  $Q$  with the above mentioned methods, we can conclude that the LSAD method is more robust and more precise for  $Q$  estimation than the other two methods.

### Effect of bandwidth

As is well known, it is significant for  $Q$  estimation to select an optimal frequency band, which has a high signal-to-noise ratio (S/N) from noisy data. However, sometimes it is tough to determine the so-called optimal frequency band. For that reason, we analyze the effect of the frequency band selection on  $Q$  estimation by our means. In this test, we use the second trace ( $Q = 40$ ) of the synthetic attenuation model (Figure 2a), and we assume that the density can be obtained accurately exactly. The time window width is 70 ms. A 5% Gaussian random noise is added to the noise-free

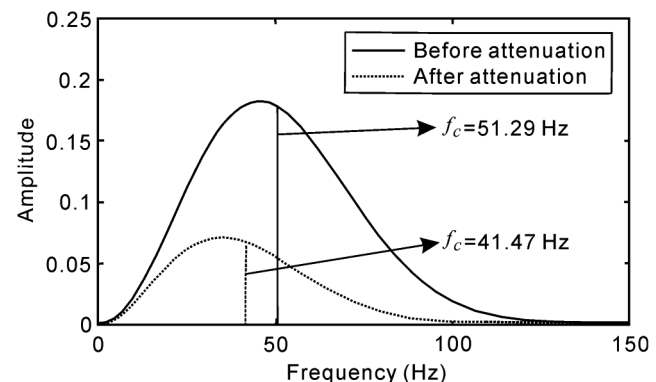


Figure 9. The spectrums before and after attenuation corresponding to the second trace ( $Q = 40$ ) of the synthetic attenuation model.

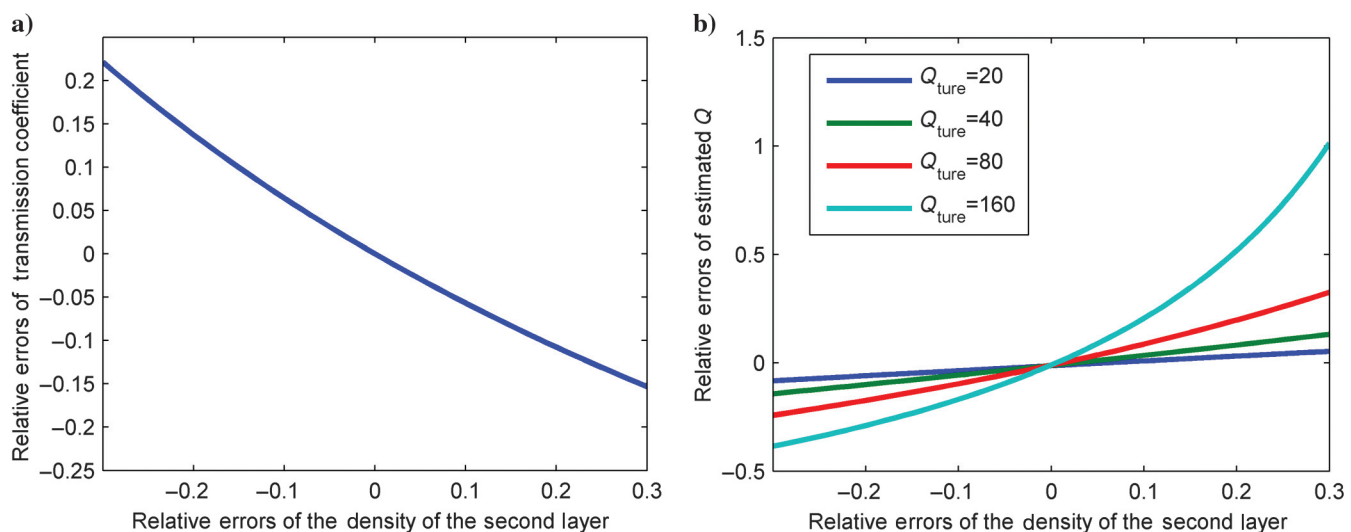


Figure 8. (a) The corresponding relative errors of the transmission coefficient caused by the computed density of the second layer. (b) The relative errors of the estimated  $Q$ .

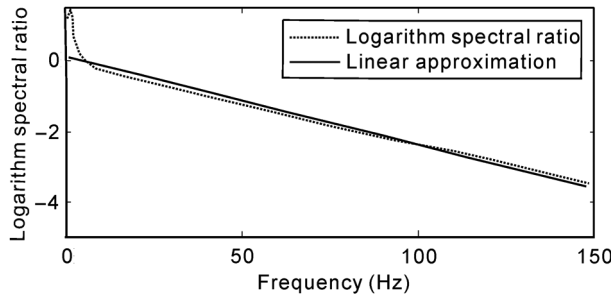


Figure 10. The logarithmic spectrum ratio calculated from the spectrums in Figure 9.

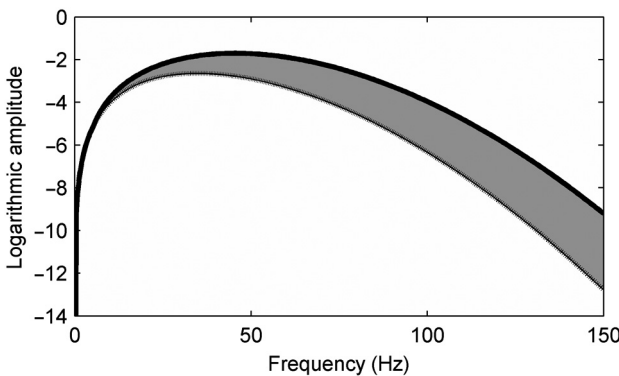


Figure 11. The LSAD.

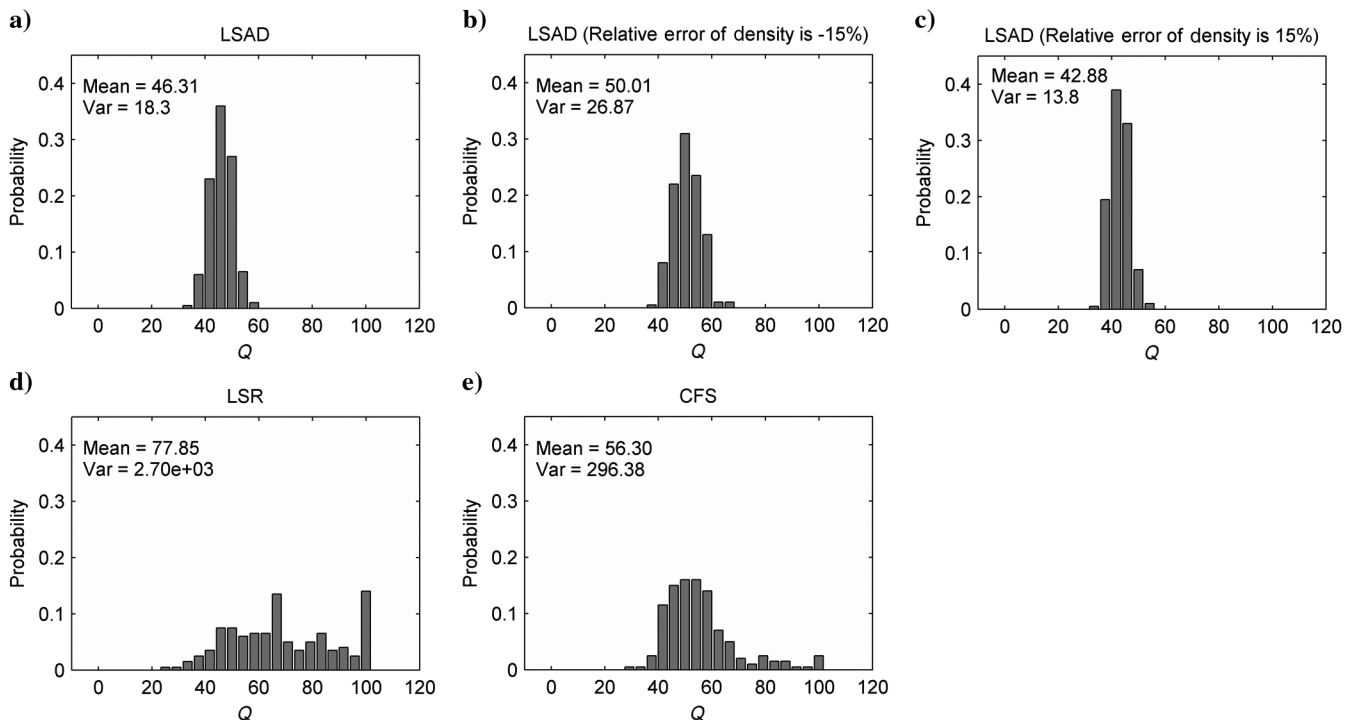


Figure 12. Histograms of the estimated  $Q$  with different methods when the additive Gaussian random noise is 5%. (a) LSAD method with accurate transmission coefficient. (b) LSAD method with  $-15\%$  relative error. (c) LSAD method with  $15\%$  relative error. (d) LSR method. (e) CFS method.

trace. A series of frequency bands, whose starting frequencies are either 5 or 10 Hz and ending frequencies are different, are chosen to estimate  $Q$  factors. Figure 15 depicts the estimated  $Q$  with three different  $Q$  estimation methods mentioned before using different frequency bands. Figure 16 displays the performance of these approaches when 10% Gaussian random noise is added. From Figures 15 and 16, we can see that the LSAD method is insensitive to the frequency band and gives better results than the other two methods; thus, the selection of the frequency band is not strict. On the contrary, CFS method and LSR method depend much on bandwidth, particularly for the LSR method. And we must be careful when selecting the frequency band for the LSR method, to obtain a reliable result.

### Effect of time window width

Before estimating  $Q$  from the seismic data, we should extract the signals by the time window from the record. To figure out how the width of time window will influence  $Q$  estimation, we design a test in this part. A rectangular time window is taken to extract the wavelet, as shown in Figure 17. The second trace ( $Q = 40$ ) of the synthetic attenuation model (Figure 2a) is used again. We assume that the density can be obtained accurately. Then, we evaluate  $Q$  by three  $Q$  estimation methods using different widths of time window and the results are indicated in Figure 18. It is explicit that the width selection of the time window almost has little effect on the LSAD method for  $Q$  estimation. In contrast, the LSR and CFS methods are sensitive to the width of the time window. Especially, when the time

***Q* factor estimation with LSAD**

V165

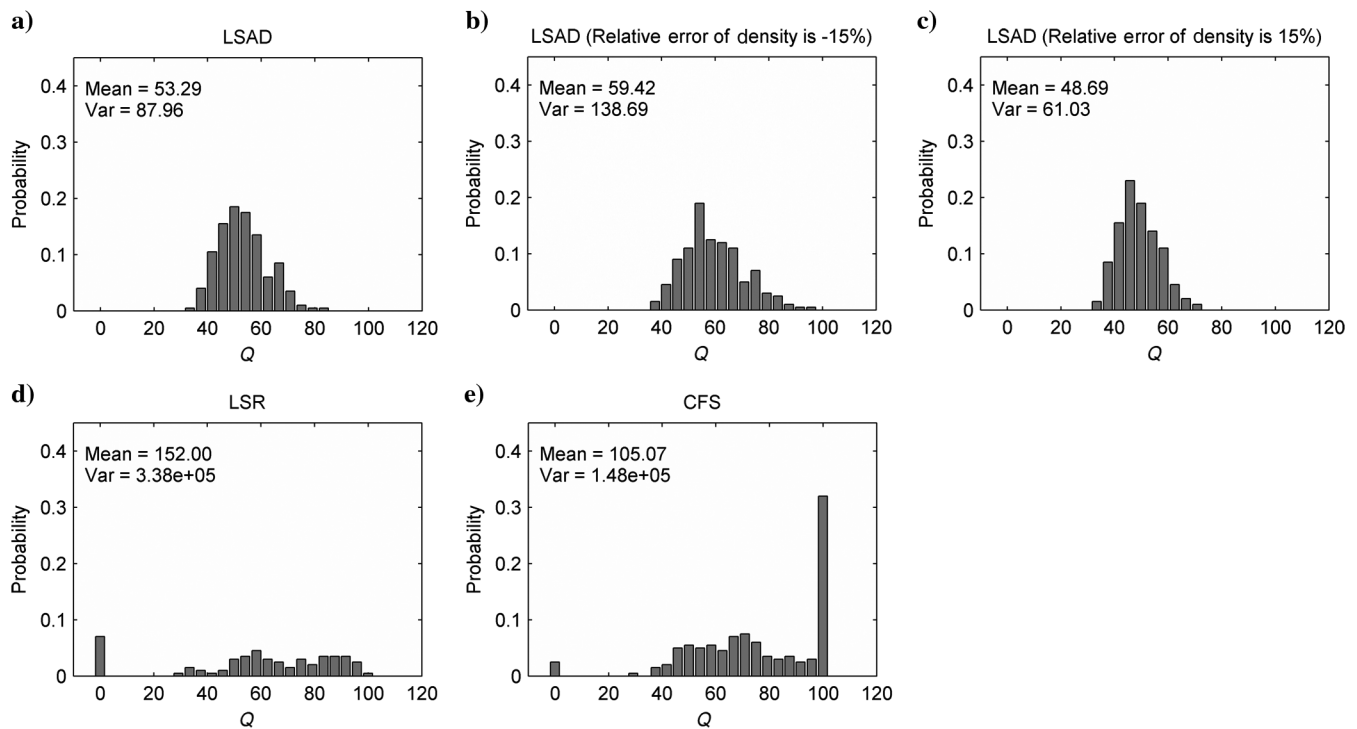


Figure 13. Histograms of the estimated  $Q$  with different methods when the additive Gaussian random noise is 10%. (a) LSAD method with accurate transmission coefficient. (b) LSAD method with  $-15\%$  relative error. (c) LSAD method with  $15\%$  relative error. (d) LSR method. (e) CFS method.

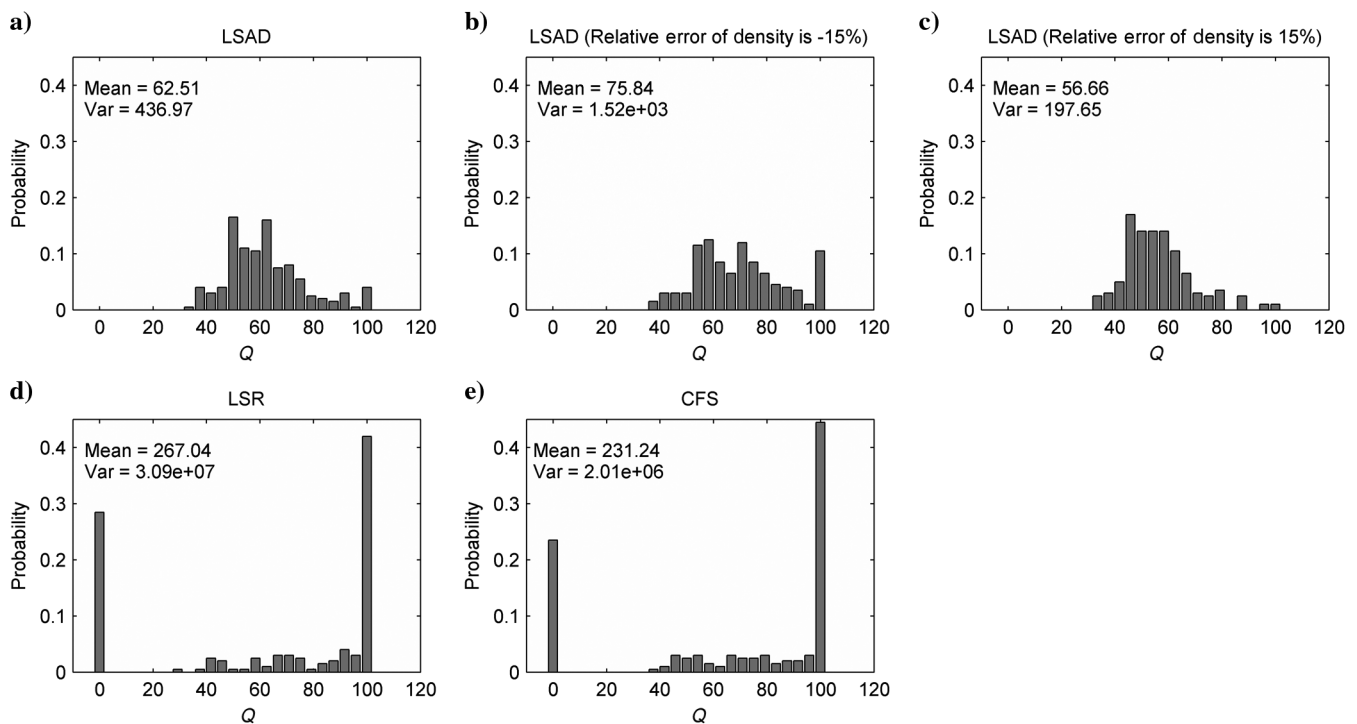


Figure 14. Histograms of the estimated  $Q$  with different methods when the additive Gaussian random noise is 15%. (a) LSAD method with accurate transmission coefficient. (b) LSAD method with  $-15\%$  relative error. (c) LSAD method with  $15\%$  relative error. (d) LSR method. (e) CFS method.

Figure 15. The estimated  $Q$  with three different  $Q$  estimation methods mentioned above using different frequency bands when 5% Gaussian random noise was added to the noise-free trace. (a) The starting frequency is 5 Hz. (b) The starting frequency is 10 Hz.

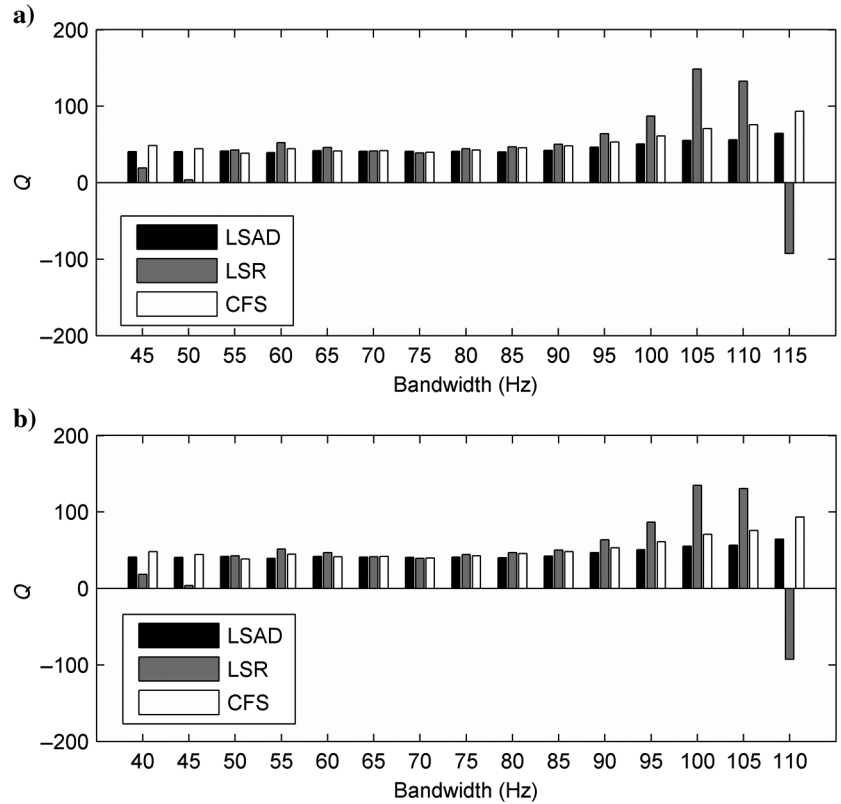
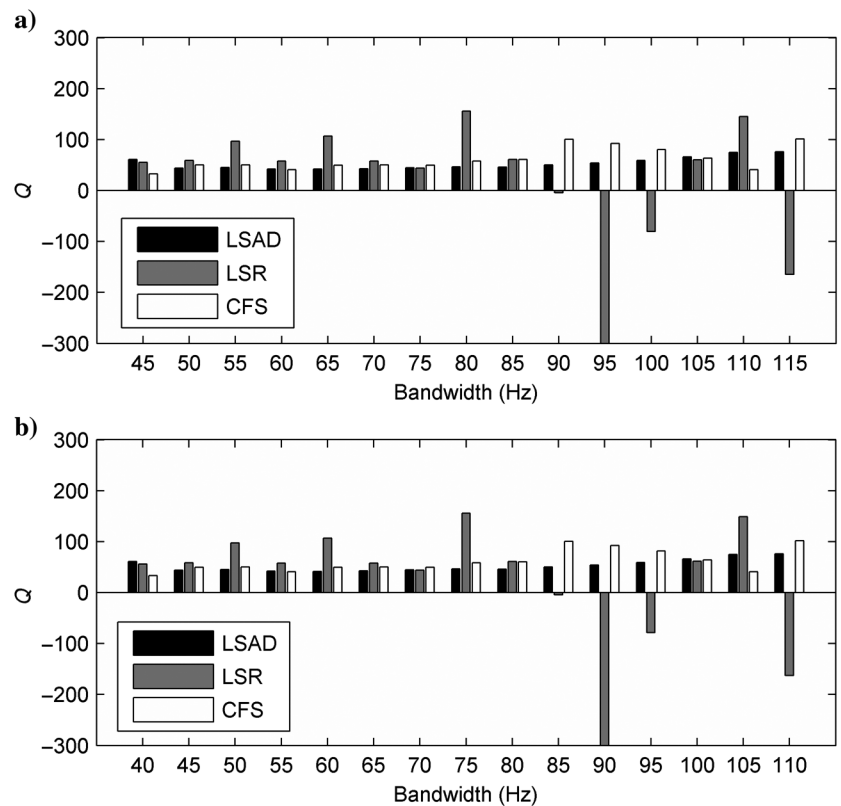


Figure 16. The estimated  $Q$  with three different  $Q$  estimation methods mentioned above using different frequency bands when 10% Gaussian random noise was added to the noise-free trace. (a) The starting frequency is 5 Hz. (b) The starting frequency is 10 Hz.



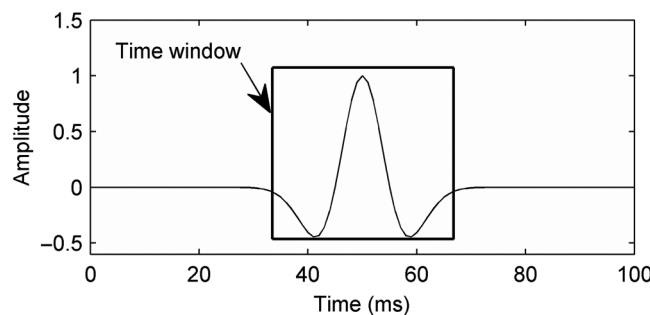


Figure 17. A rectangular time window used to extract the wavelet.

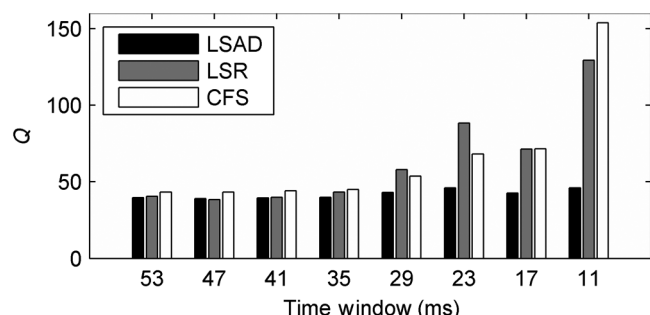


Figure 18. The estimated  $Q$  with three  $Q$  estimation methods using various widths of the time window.

Table 1. Model parameters.

Layer	Thickness (m)	Velocity (m/s)	Density ( $\text{g}/\text{cm}^3$ )	$Q$ factor
1	200	2500	2.1920	40
2	200	3000	2.2943	60
3	200	2000	2.0731	20
4	200	3500	2.3844	80
5	200	4500	2.5390	100

window is relatively narrow, both methods have large estimation errors.

#### Comparison of three $Q$ estimation methods from zero-offset VSP data

We give a further comparison of these three  $Q$  estimation methods mentioned above from zero-offset VSP data. A four-layer model is given, and the parameters of this model are shown in Table 1. For VSP data modeling, a point source is located at  $(0, 0)$ , and the source is a Ricker wavelet with the dominant frequency 30 Hz. The receivers are spread from 0 to 1000 m with a 20-m interval along the  $z$ -direction. Then, a synthetic zero-offset VSP data with attenuation, is modeled using the finite-difference method in the frequency domain by replacing the real-valued velocity with a complex-valued velocity (Marfurt, 1984; Song et al., 1995; Hicks and Pratt, 2001), as shown in Figure 19a. And Figure 19b is the case of all traces of the VSP data containing random noise of 0.2% of the maximum amplitude of the reference wavelet at depth 0 m.

For the synthetic zero-offset VSP data in the absence of noise, we can isolate the first arrivals of the VSP data with a time window. The selected frequency band of these three methods is 10–100 Hz. In the

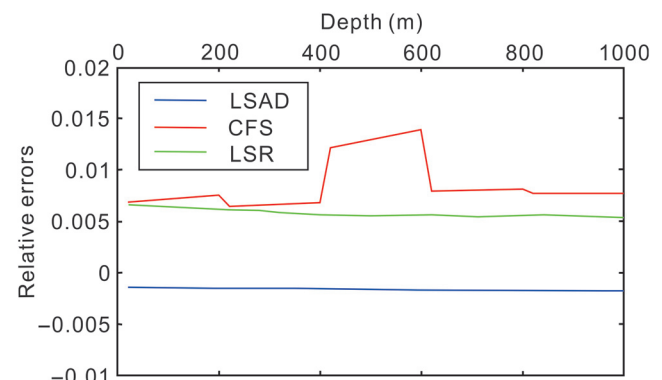


Figure 20. The relative errors of estimated  $Q$  using the first arrivals of synthetic zero-offset VSP data by three different methods. The LSAD, CFS, and LSR are displayed in blue, red, and green, respectively.

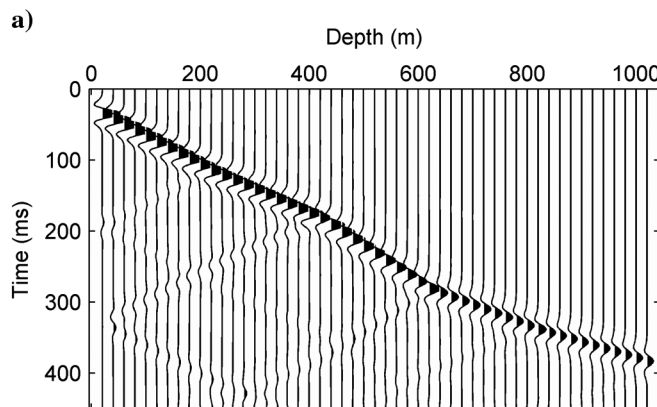
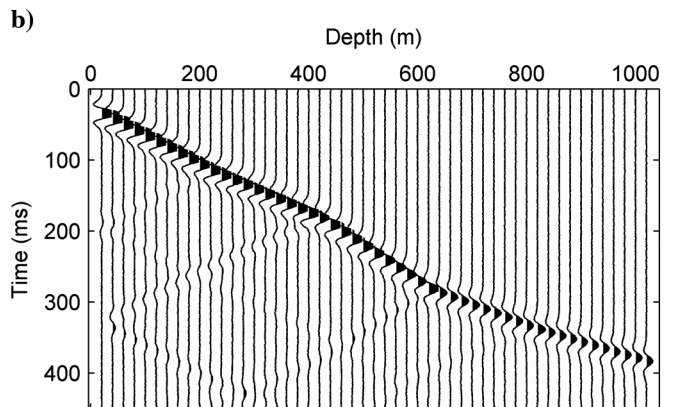


Figure 19. (a) The noise-free synthetic zero-offset VSP data with attenuation. (b) The slightly noisy synthetic zero-offset VSP data with attenuation.



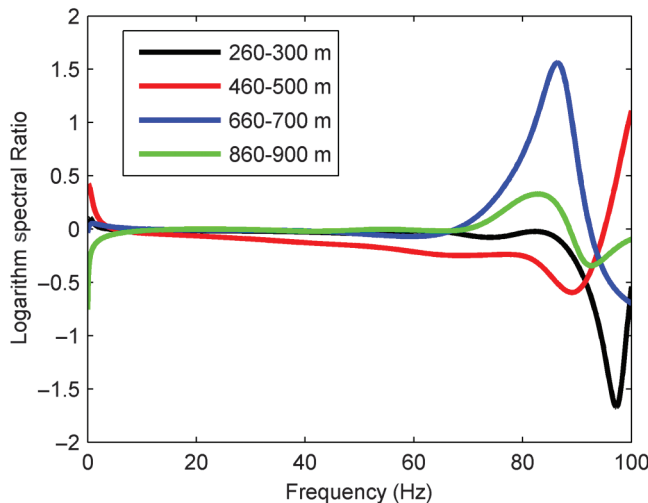


Figure 21. The logarithmic spectrum ratio of four different intervals: 260–300, 460–500, 660–700, and 860–900 m.

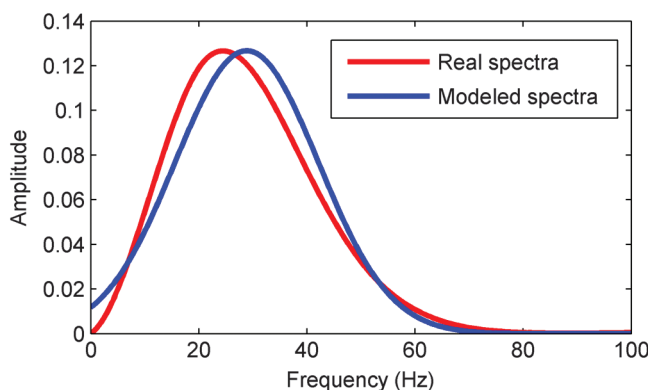


Figure 22. The real spectra and the modeled CFS spectra (the red curve) with 0–100 Hz bandwidth for the wavelet at the depth 900 m.

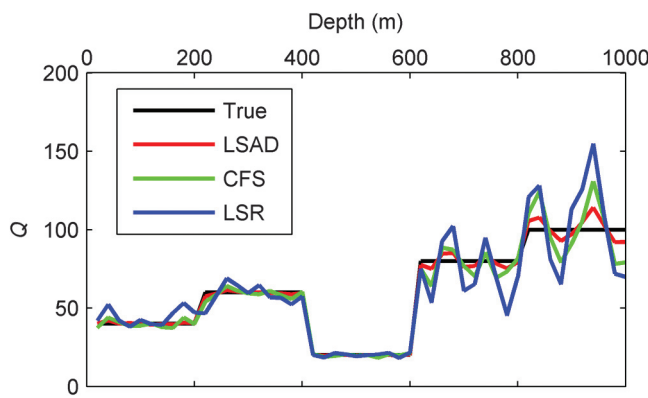


Figure 23. The relative errors of estimated  $Q$  using the first arrivals of synthetic zero-offset VSP data by three different methods. LSAD, CFS, and LSR are displayed in red, green, and blue, respectively.

process of  $Q$  measurements, the location of the shallowest receiver is regarded as a reference level, from which the average  $Q$  values that are later converted to interval  $Q$  values are obtained. And the relative errors of estimated  $Q$  by these methods are displayed in Figure 20. According to Figure 20, LSAD has the minimum relative errors among all the methods. And the relative errors of CFS are maximum, which is caused by the assumption that the incident wavelet is Gaussian in shape.

A suitable frequency band should be selected when we estimate  $Q$  from the noisy VSP data. Figure 21 shows the logarithmic spectrum ratio for the bandwidth 0–100 Hz for four different intervals: 260–300, 460–500, 660–700, and 860–900 m. We can see that the frequency band 10–65 Hz, these curves can be approximated with the linear function. Meanwhile, a modeled CFS spectrum (the red curve) with 0–100 Hz bandwidth for the wavelet at the depth 900 m is shown in Figure 22. The modeled CFS spectrum matches the real spectrum (the blue curve in Figure 22) well in the bandwidth 10–65 Hz. Therefore, this bandwidth was used for  $Q$  estimation. Figure 23 depicts the estimated  $Q$  factors by three different methods. It is obvious that all three methods show good performance for  $Q$  estimation in the shallow stratum, where the data have a high S/N. However, for the data in the deep layers with relatively low S/N, the estimated  $Q$  factors with the LSAD method (red line) match the true model (black line) better than any other methods. It also indicates that the noise immunity of LSAD is better than LSR and CFS from this comparison using zero-offset VSP data.

## APPLICATION TO FIELD DATA

Finally, our method is applied to real zero-offset VSP data. Figure 24a displays the real VSP data offered by an oil field in western China, recorded at a depth range of 2300–4260 m with a regular depth interval 20 m. The type of source is vibroseis, and it is a single source per cable position. The horizontal offset between the source and the borehole is 50 m. Figure 24b shows the downgoing wavefield of the VSP data after preprocessing (i.e., compensating for the source fired several times as the receiver is moved up the well, spherical divergence correction, denoising by band-pass filtering, and wavefield separation by  $f$ - $k$  filtering). Figure 25a displays the layered velocities calculated from manually picked first arrivals. The densities were calculated by the Gardner equation, and the obtained profile of the transmission coefficients are shown in Figure 25b and 25c, respectively. The average- $Q$  factors estimated using LSAD from the shallowest geophone is shown in Figure 25d, and the interval- $Q$  factors calculated by the average- $Q$  is shown in Figure 25e. Figure 25f shows the estimated interval- $Q$  after median filtering (seven points were used).

$Q$  factors can be calculated with the empirical equation, which is  $\frac{1}{Q} = \left(\frac{C}{v_p}\right)^2$ , where  $v_p$  is the primary velocity and  $C$  is a constant (Waters, 1978; Uddias, 1999). In addition, Li (1993) analyzes a large amount of results on  $Q$  estimation and establishes an empirical formula that explains a relation between the  $Q$  factor and primary velocity. The empirical formula is  $Q = 14v_p^{2.2}$ , where  $v_p$  is the primary velocity. Moreover, Blas (2012) uses the correlation between  $Q$  and velocity to examine whether the estimated  $Q$  is reasonable. In Figure 25f, the red line stands for the estimated interval- $Q$ , and the blue line stands for the layered velocities, which shows a good correlation between estimated interval- $Q$  and interval velocities.

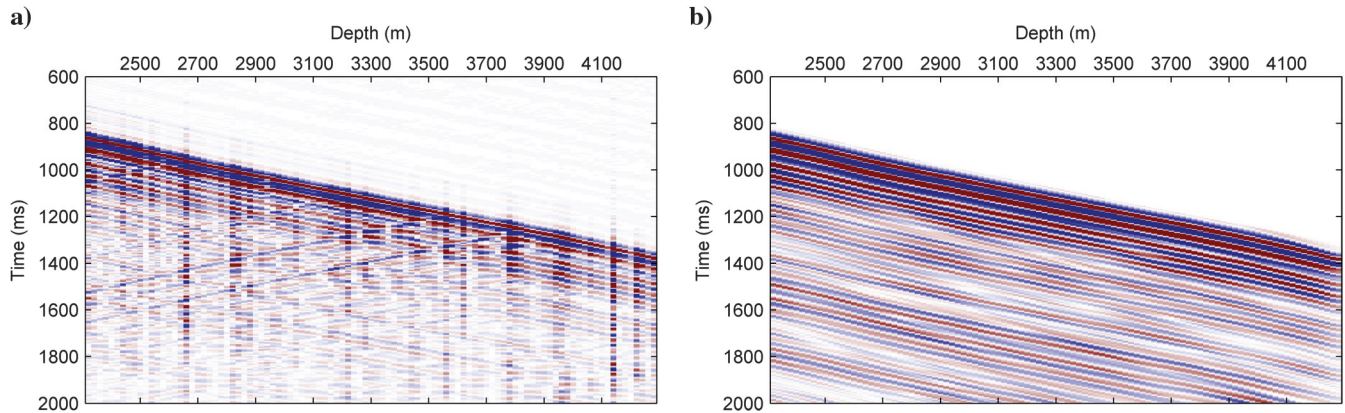


Figure 24. (a) A real zero-offset VSP data. (b) The downgoing wavefield after preprocessing.

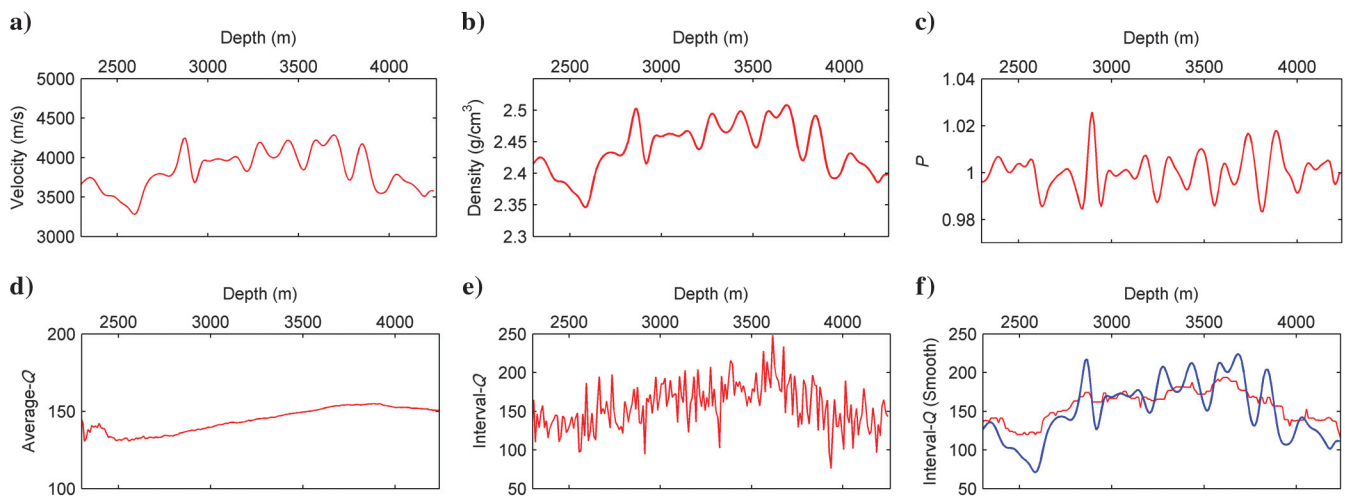


Figure 25. (a) The layered velocity obtained from the first arrivals. (b) The calculated density using the Gardner equation. (c) The calculated transmission coefficient  $P$ . (d) Estimated average- $Q$  factors based on LSAD. (e) Estimated interval- $Q$  factors from average- $Q$ . (f) Estimated interval- $Q$  factors after median filtering.

## CONCLUSIONS

In this paper, we present a novel  $Q$  estimation method on the basis of the variation of the logarithmic spectral area of the seismic wave, in which amplitude loss due to energy partitioning from transmission is considered. Effectiveness and noise-immunity analysis on LSAD confirms that the proposed method is valid for  $Q$  estimation and has good noise immunity to different types of random noise. Although there may exist error for calculated density using the Gardner equation, it is fortunately found that this kind of error has a quite slight influence on the accuracy of  $Q$  estimation when the relative error of density is in the range of  $-15\%$  to  $15\%$ , and that the stronger the attenuation is, the method is less sensitive to density.

For purposes of testing the properties of our method from more aspects, we conduct further comparative analysis of the noise immunity, bandwidth, and time window among our method and another two common methods, namely, LSR and CFS. From the analyses, we can come to the following conclusions: The LSAD method is more robust than the other two methods for  $Q$  estimation with the data including Gaussian random noise and the LSAD

method is less sensitive to the bandwidth and time window than the other two methods. Finally, we apply our method to real VSP data, and the evaluated  $Q$  shows good relevance to interval velocity, which convincingly proves the validity of the presented approach.

Even though the LSAD method is very effective against random noise, its robustness will be reduced in the presence of spectral interference. For VSP data, the spectrum of direct wave may be affected by the upgoing wave, which fortunately can be reduced by wavefield separation. However, if we want to measure  $Q$  stably based on the LSAD method for reflection seismic data, further research, combining the LSAD method with a variable-window time-frequency analysis transform or well-log-based localized spectral correction, should be done to adapt the LSAD to reflection seismic data.

## ACKNOWLEDGMENTS

This research is supported by the National Natural Science Foundation of China (grant no. 41274137), the National Science and

Technology of Major Projects of China (grant no. 2011ZX05023-005-005), and the National Engineering Laboratory of Offshore Oil Exploration. We would also like to thank the reviewers of this paper for their excellent suggestions.

## APPENDIX A ERROR ANALYSIS

Equation 9 can be rewritten as a generic form

$$y = a + b\omega, \quad (\text{A-1})$$

where  $y = \ln[A(z_{i+1}, \omega)] - \ln[A(z_i, \omega)]$ ,  $a = \ln(P_i)$ ,  $b = -\frac{\Delta t_i}{2Q}$  is the parameter to be estimated (from which the  $Q$  factor can be derived). Equation A-1 is correct for all  $\omega$ . Let us suppose  $\omega = \omega_j, j = 1, 2, \dots, m$ . Equation A-1 can be written as the discrete form

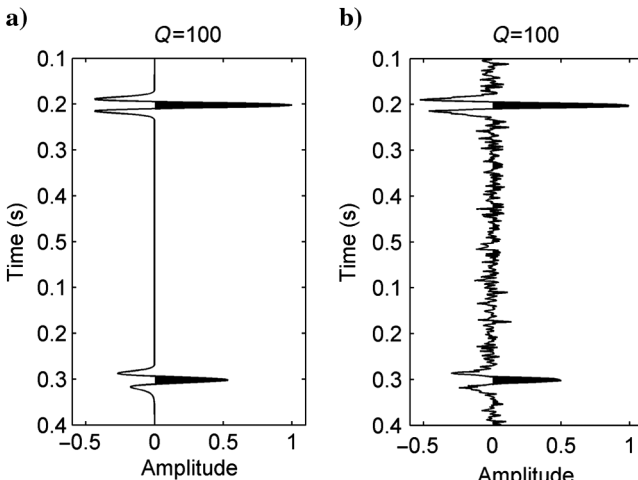


Figure A-1. Synthetic seismic data with  $Q = 100$ . (a) Noise-free case. (b) Case of 5% random noise data.

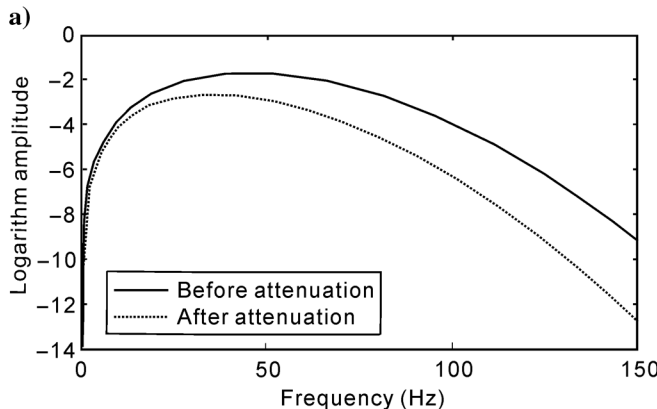


Figure A-2. The logarithmic spectrum corresponding to  $Q = 100$ . The solid line is the logarithmic spectrum of wavelet before attenuation, and the dotted line is the logarithmic spectrum of wavelet after attenuation. (a) Noise-free case. (b) Case of 5% random noise.

$$y_j = a + b\omega_j. \quad (\text{A-2})$$

We also use  $\epsilon_j$  to denote the error that comes into the data  $y_j$ , and assuming that there is no error in  $a$ . In the noise condition, equation A-2 become

$$y_j + \epsilon_j = a + b\omega_j \quad j = 1, 2, \dots, m. \quad (\text{A-3})$$

According to the LSAD method, we have

$$\begin{aligned} b^{\text{LSAD}} &= \frac{\sum_{j=1}^m (y_j - a + \epsilon_j)}{\sum_{j=1}^m \omega_j} \\ &= \frac{\sum_{j=1}^m (y_j - a)}{\sum_{j=1}^m \omega_j} + \frac{\sum_{j=1}^m \epsilon_j}{\sum_{j=1}^m \omega_j} \\ &= b^{\text{True}} + \frac{\sum_{j=1}^m \epsilon_j}{\sum_{j=1}^m \omega_j}, \end{aligned} \quad (\text{A-4})$$

where  $b^{\text{LSAD}}$  denotes the  $b$  estimated by LSAD,  $b^{\text{True}}$  is the true value of  $b$ . If the noise has zero mean in the logarithmic spectral domain, then  $\sum_{j=1}^m \epsilon_j = 0$ , and we obtain  $b^{\text{LSAD}} = b^{\text{True}}$ .

Next, we give an analysis on the noise immunity of the LSAD method by a numerical experiment. Figure A-1a shows a single attenuation trace with  $Q = 100$ , and Figure A-1b is the case of 5% Gaussian random noise. The corresponding logarithmic spectrums with and without noise are shown in Figure A-2. Meanwhile, Table A-1 displays the logarithmic spectral area and the LSAD com-

**Table A-1. The logarithmic spectral area and the LSAD.**

	Data without noise	Data with 5% random noise
Logarithmic spectral area before attenuation	-214.7	-223.7
Logarithmic spectral area after attenuation	-261.6	-269.6
LSAD	46.9	45.9

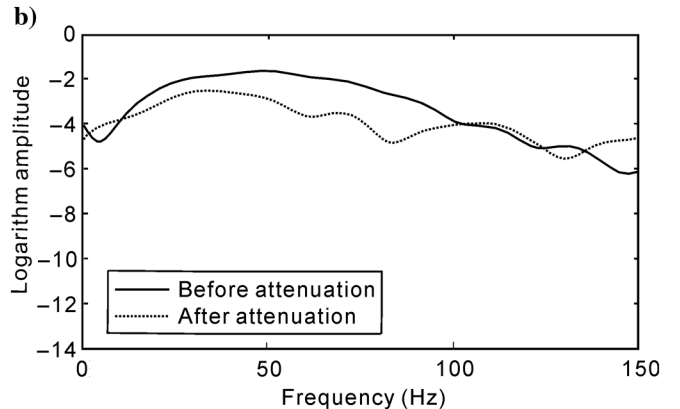


Figure A-2. The logarithmic spectrum corresponding to  $Q = 100$ . The solid line is the logarithmic spectrum of wavelet before attenuation, and the dotted line is the logarithmic spectrum of wavelet after attenuation. (a) Noise-free case. (b) Case of 5% random noise.

puted from Figure A-2, with the selected frequency band of 10–100 Hz. Comparing the LSAD in the noise-free case with that in the case of 5% random noise, we surprisingly find almost no changes in the LSAD. The sum of errors,  $\sum_{j=1}^m \epsilon_j = 1.0$ , is very close to zero, which demonstrates that our method has good noise immunity. This can also explain why the LSAD method is robust even though the data include strong random noise. Moreover, the estimated  $Q$  factor based on the LSAD method is 99.8 for data without noise, and the estimated  $Q$  is 104.5 for data with 5% random noise, which further demonstrates the robustness of LSAD method in the strong random noise interference situation.

## REFERENCES

- Best, A., 1997, The effect of pressure on ultrasonic velocity and attenuation in near-surface sedimentary rocks: *Geophysical Prospecting*, **45**, 345–364, doi: [10.1046/j.1365-2478.1997.00344.x](https://doi.org/10.1046/j.1365-2478.1997.00344.x).
- Blías, E., 2012, Accurate interval  $Q$ -factor estimation from VSP data: *Geophysics*, **77**, no. 3, WA149–WA156, doi: [10.1190/geo2011-0270.1](https://doi.org/10.1190/geo2011-0270.1).
- Clark, R. A., A. J. Carter, P. C. Nevill, and P. M. Benson, 2001, Attenuation measurements from surface seismic data — Azimuthal variation and time-lapse case studies: 63rd Annual International Conference and Exhibition, EAGE, Extended Abstracts, L-28.
- Futterman, W. I., 1962, Dispersive body waves: *Journal of Geophysical Research*, **67**, 5279–5291, doi: [10.1029/JZ067i013p05279](https://doi.org/10.1029/JZ067i013p05279).
- Gardner, G. H. F., L. W. Gardner, and A. R. Gregory, 1974, Formation velocity and density — The diagnostic basics for stratigraphic traps: *Geophysics*, **39**, 770–780, doi: [10.1190/1.1440465](https://doi.org/10.1190/1.1440465).
- Hackert, C. L., and J. O. Parra, 2004, Improving  $Q$  estimates from seismic reflection data using well-log-based localized spectral correction: *Geophysics*, **69**, 1521–1529, doi: [10.1190/1.1836825](https://doi.org/10.1190/1.1836825).
- Hicks, G. J., and R. G. Pratt, 2001, Reflection waveform inversion using local descent methods: Estimating attenuation and velocity over a gas-sand deposit: *Geophysics*, **66**, 598–612, doi: [10.1190/1.1444951](https://doi.org/10.1190/1.1444951).
- Johnston, D. H., M. N. Toksoz, and A. Timur, 1979, Attenuation of seismic waves in dry and saturated rocks: II. Mechanisms: *Geophysics*, **44**, 691–711, doi: [10.1190/1.1440970](https://doi.org/10.1190/1.1440970).
- Li, Q., 1993, The road of accurate exploration: Petroleum Industry Press (in Chinese).
- Liao, Q., and G. A. McMechan, 1996, Multifrequency viscoacoustic modeling and inversion: *Geophysics*, **61**, 1371–1378, doi: [10.1190/1.1444060](https://doi.org/10.1190/1.1444060).
- Malinowski, M., S. Operto, and A. Ribodetti, 2011, High-resolution seismic attenuation imaging from wide-aperture onshore data by visco-acoustic frequency-domain full-waveform inversion: *Geophysical Journal International*, **186**, 1179–1204, doi: [10.1111/j.1365-246X.2011.05098.x](https://doi.org/10.1111/j.1365-246X.2011.05098.x).
- Marfurt, K. J., 1984, Accuracy of finite-difference and finite-element modeling of the scalar and elastic wave equations: *Geophysics*, **49**, 533–549, doi: [10.1190/1.1441689](https://doi.org/10.1190/1.1441689).
- Maultzsch, S., M. Chapman, E. Liu, and X. Li, 2007, Modelling and analysis of attenuation anisotropy in multi-azimuth VSP data from the Clair field: *Geophysical Prospecting*, **55**, 627–642, doi: [10.1111/j.1365-2478.2007.00645.x](https://doi.org/10.1111/j.1365-2478.2007.00645.x).
- Mittet, R., R. Sollie, and K. Hokstad, 1995, Prestack depth migration with compensation for absorption and dispersion: *Geophysics*, **60**, 1485–1494, doi: [10.1190/1.1443882](https://doi.org/10.1190/1.1443882).
- Quan, Y., and J. M. Harris, 1997, Seismic attenuation tomography using the frequency shift method: *Geophysics*, **62**, 895–905, doi: [10.1190/1.1444197](https://doi.org/10.1190/1.1444197).
- Rao, Y., and Y. Wang, 2009, Fracture effects in seismic attenuation images reconstructed by waveform tomography: *Geophysics*, **74**, no. 4, R25–R34, doi: [10.1190/1.3129264](https://doi.org/10.1190/1.3129264).
- Reine, C., R. A. Clark, and M. van der Baan, 2012a, Robust prestack  $Q$ -determination using surface seismic data: Part 1. Method and synthetic examples: *Geophysics*, **77**, no. 1, R45–R56, doi: [10.1190/geo2011-0073.1](https://doi.org/10.1190/geo2011-0073.1).
- Reine, C., R. A. Clark, and M. van der Baan, 2012b, Robust prestack  $Q$ -determination using surface seismic data: Part 2. 3D case study: *Geophysics*, **77**, no. 1, B1–B10, doi: [10.1190/geo2011-0074.1](https://doi.org/10.1190/geo2011-0074.1).
- Reine, C., M. van der Baan, and R. A. Clark, 2009, The robustness of seismic attenuation measurements using fixed and variable-window time-frequency transforms: *Geophysics*, **74**, no. 2, WA123–WA135, doi: [10.1190/1.3043726](https://doi.org/10.1190/1.3043726).
- Song, Z., and P. R. Williamson, 1995, Frequency-domain acoustic-wave modeling and inversion of crosshole data: Part 1. 2.5-D modeling method: *Geophysics*, **60**, 784–795, doi: [10.1190/1.1443817](https://doi.org/10.1190/1.1443817).
- Tonn, R., 1991, The determination of the seismic quality factor  $Q$  from VSP data: A comparison of different computational methods: *Geophysical Prospecting*, **39**, 1–27, doi: [10.1111/j.1365-2478.1991.tb00298.x](https://doi.org/10.1111/j.1365-2478.1991.tb00298.x).
- Udias, A., 1999, Principles of seismology: Cambridge University Press.
- Wang, Y., 2002, A stable and efficient approach of inverse  $Q$  filtering: *Geophysics*, **67**, 657–663, doi: [10.1190/1.1468627](https://doi.org/10.1190/1.1468627).
- Wang, Y., 2004,  $Q$  analysis on reflection seismic data: *Geophysical Research Letters*, **31**, L17606, doi: [10.1029/2004GL020572](https://doi.org/10.1029/2004GL020572).
- Wang, Y., 2006, Inverse  $Q$ -filter for seismic resolution enhancement: *Geophysics*, **71**, no. 3, V51–V60, doi: [10.1190/1.2192912](https://doi.org/10.1190/1.2192912).
- Waters, K. H., 1978, Reflection seismology: John Wiley and Sons, Inc.
- Winkler, K. W., and A. Nur, 1982, Seismic attenuation — Effects of pore fluids and frictional sliding: *Geophysics*, **47**, 1–15, doi: [10.1190/1.1441276](https://doi.org/10.1190/1.1441276).
- Zhang, C., and T. J. Ulrych, 2002, Estimation of quality factors from CMP records: *Geophysics*, **67**, 1542–1547, doi: [10.1190/1.1512799](https://doi.org/10.1190/1.1512799).